Adsorption 7: 91–103, 2001

Adsorption Equilibrium and Dynamics of Methyl Iodide in a Silver Ion-Exchanged Zeolite Column at High Temperatures

BYUNG SEON CHOI*, GEUN IL PARK AND JOON HYUNG KIM
Korea Atomic Energy Research Institute, Yusung P.O. Box 105, Taejon, Korea
bschoi@kaeri.re.kr

JAE WOOK LEE
Department of Chemical Engineering, Seonam University, Namwon 590-711, Korea

SEUNG KON RYU
Department of Chemical Engineering, Chungnam National University, Taejon 305-704, Korea

Received May 26, 2000; Revised February 12, 2001; Accepted March 28, 2001

Abstract. An extensive evaluation was carried out to determine the optimal silver ion-exchanged level for the removal of methyl iodide at high temperatures up to 400°C. Based on the degree of silver utilization, the optimal silver loading and temperature were about 10 wt% and 175°C, respectively. The physical and chemical properties of silver ion-exchanged zeolite were characterized by instrumental analysis such as BET, TG/DTA and SEM-EDS. Adsorption dynamics was also studied at different temperatures, and methyl iodide concentrations. A simple dynamic model was formulated by employing the linear driving force (LDF) approximation inside adsorbent particles, and the nonisothermal Langmuir-Freundlich equation. The model equations were solved numerically by an orthogonal collocation method. The proposed dynamic model satisfactorily simulated the experimental breakthrough results.

Keywords: high temperature, methyl iodide, silver ion-exchanged zeolite, adsorption equilibrium, dynamic model

Introduction

For the several years, emphasis has been placed on the reduction of radioactive gaseous waste released from nuclear facilities. Of the radioactive wastes, radioiodines such as elemental iodines (I, I_2), organic iodide (CH_3I) and hypoiodous acid (HOI) are the most important nuclides due to their volatility and the significant radiological effects on human body and environment (Wren et al., 1999; Funabashi et al., 1995). Controlling the release of these species depends on the design of the off-gas treatment and ventilation systems within each particular process of a nuclear power plant and also on the reactor type.

Various technologies have been addressed and developed over the past decades to control the discharge of iodine to the environment. Liquid scrubbing systems utilizing caustic, nitric acid, and mercury have been studied (Pence and Staples, 1974). The use of solid adsorbents has also been investigated for the main removal system or as back-up or polishing systems following one of the liquid scrubbing systems. The removal of radioiodines has generally been performed using activated carbon (Wren et al., 1999; Deitz and Jonas, 1978; Marin et al., 1991), silica (Modolo and Odoj, 1997), alumina (Funabashi et al., 1995), and

*To whom correspondence should be addressed.

polymeric resin. Also, impregnants such as KI, TEDA (triethylene diamine), and silver have been widely used to improve the removal efficiency.

Although activated carbon has been successfully used in nuclear power plants, it cannot be considered as a primary adsorbent in a high temperature system, because of its low ignition temperature and its adverse reaction with nitrogen oxide. Therefore, activated carbon is virtually ruled out for high temperature systems like the DUPIC (Direct Use of Spent PWR Fuel In CANDU Reactor) process. As a result, the promising approach to the problem of iodine removal under high temperature conditions is to use inorganic adsorbents in which a stable iodine compound is formed. Numerous studies for the removal of radioiodine from the off-gas stream of nuclear facilities have been performed with various silver ion-exchanged inorganic adsorbents (Jubin, 1994; Modolo and Odoj, 1997; Funabashi et al., 1995; Thomas et al., 1977). Compared with the wet processes, these systems in which adsorbents function as the primary filtering of radioiodine have some advantages in their simplicity and smaller amounts of secondary radioactive wastes. A number of studies have been conducted to evaluate the loading of both elemental and methyl iodide on silver ion-exchanged zeolite at high temperature. These studies focused primarily on the macro-scale of the deep-bed during the evaluation of the material under a broad range of process conditions and contaminants for total bed loading at the time of breakthrough. A few studies have evaluated the equilibrium and maximum loading capacities of silver ion-exchanged zeolite (Jubin, 1994). In our laboratory, preliminary performance tests for the removal of methyl iodide by various silver ion-exchanged adsorbents had already been carried out (Choi et al., 1997). However, more detailed studies are needed to establish silver utilization for the removal of radioiodine as a function of process temperature. Methyl iodide was chosen as a representative of the organic iodides existing in the containment vessel of a power reactor because it is considered to be one of the most difficult species to remove among the organic iodides, compared to elemental iodine (Kovach, 1981).

The objectives of this paper are to evaluate the adsorption and dynamic characteristics of gaseous methyl iodide on silver ion-exchanged zeolites at high temperatures up to 400°C. From the standpoint of silver utilization for the removal of methyl iodide, both the optimal operating temperature and the effective silver ion-exchanged level were determined. The physical and chemical properties of silver ion-exchanged zeolite before and after adsorption were characterized by instrumental analysis, namely BET, TG/DTA, and SEM-EDS. The reliability of an adsorption process model largely depends on the adequacy of its constituent models, which represent the equilibrium isotherm, mass transfer, and heat transfer dynamics (Ruthven, 1984; Yang, 1987; Ruthven et al., 1994). In this study, a simple nonisothermal and axially dispersed plug-flow model is adopted to simulate the experimental breakthrough curves. The Langmuir-Freundlich isotherm model is used to represent the equilibrium relationship, and the linear driving force (LDF) approximation is used to represent the particle uptake.

Theoretical Approach

Model Description

For a single component nonisothermal and isobaric adsorption process in a packed bed of adsorbent, the equation for the dimensionless material balance is as follows, assuming axially dispersed plug-flow and ideal gas law behavior for the gas-phase.

$$\frac{\partial X}{\partial \tau} = \frac{1}{P_{em}}\left(\frac{\partial^2 X}{\partial \chi^2} - \frac{2}{\theta}\frac{\partial X}{\partial \chi}\frac{\partial \theta}{\partial \chi}\right) - V\frac{\partial X}{\partial \chi} + \varphi(X-1)\frac{\partial Y}{\partial \tau} \tag{1}$$

The dimensionless total material balance is given by

$$\frac{\partial V}{\partial \chi} = \frac{1}{P_{em}}\left(\frac{2}{\theta^2}\left(\frac{\partial \theta}{\partial \chi}\right)^2 - \frac{1}{\theta}\frac{\partial^2 \theta}{\partial \chi^2}\right) + \frac{1}{\theta}\frac{\partial \theta}{\partial \tau} + \frac{V}{\theta}\frac{\partial \theta}{\partial \chi} - \varphi\frac{\partial Y}{\partial \tau} \tag{2}$$

A dimensionless energy balance for the system, with axial thermal conduction yields

$$\frac{\partial \theta}{\partial \tau} = \left(\frac{1}{P_{eh}} + \frac{\phi}{P_{em}}\right)\frac{\partial^2 \theta}{\partial \chi^2} - \phi V\frac{\partial \theta}{\partial \chi} - \frac{2\phi}{P_{em}}\frac{1}{\theta}\left(\frac{\partial \theta}{\partial \chi}\right)^2 + \phi\varphi(\theta+\zeta)\frac{\partial Y}{\partial \tau} \tag{3}$$

The boundary conditions are as follows:

$$\left.\frac{\partial X}{\partial \chi}\right|_{\chi=0} = -P_{em}(X|_{\chi=0^-} - X|_{\chi=0^+}) \tag{4}$$

$$\left.\frac{\partial X}{\partial \chi}\right|_{\chi=1} = 0 \tag{5}$$

$$V(0,\tau) = 1 \tag{6}$$

$$\left.\frac{\partial \theta}{\partial \chi}\right|_{\chi=0} = -P'_{eh}(\theta|_{\chi=0^-} - \theta|_{\chi=0^+}) \tag{7}$$

$$\left.\frac{\partial \theta}{\partial \chi}\right|_{\chi=1} = 0 \tag{8}$$

The particle uptake equation represented by the LDF approximation and the equilibrium isotherm expression completes the breakthrough model. For particle uptake, the LDF mass-transfer-rate model is given as follows:

$$\frac{\partial Y}{\partial \tau} = \alpha(Y^* - Y) \tag{9}$$

The equilibrium adsorption capacity, Y^*, in turn, is given by the equilibrium adsorption isotherm. In this study, the Langmuir-Freundlich equilibrium isotherm model is used since it provides a very good fit of experimental equilibrium data over a wide range of pressures and temperatures. The equation is given as follows:

$$Y^* = \frac{\beta X^n}{1 + \beta X^n} \tag{10}$$

where

$$\beta = b_0 \exp\left(\frac{(-\Delta H_A)}{RT_f}\frac{1}{\theta}\right) P_f^n \tag{11}$$

Numerical Solution

The dynamic equations for the gas-phase concentration, solid-phase concentration, gas velocity, as well as bed temperature given earlier were solved simultaneously to simulate the breakthrough profiles. A system of partial differential equations was numerically solved. Equations (1) and (3) were first discretized using an orthogonal collocation method (Villadsen and Michelson, 1978; Finlayson, 1972; Raghavan and Ruthven, 1983). The overall material balance was converted to a set of linear algebraic equations in order to solve for the gas velocity in the bed. In this study, there were a total of 30 collocation points, on account of the sharp concentration and temperature waves traveling down the column. The linear algebraic equations arising from the discretized overall material balance were efficiently solved using LU-decomposition. The resultant first-order equations were simultaneously integrated using an integrating package, DVODE of the International Mathematics and Science Library (IMSL).

Experimental

Manufacture of Silver Ion-Exchanged Zeolite

The sodium form zeolite (NaX) of 8–16 mesh Linde Molecular Sieves 13X (Supplied by Aldrich Co., USA) was used as a base adsorbent to prepare silver ion-exchanged zeolite, *namely AgX*. AgX was prepared through the ion exchange method in a batch reactor. Zeolite was purged with water-saturated air stream at room temperature for three days to equilibrate it with moisture, which prevents bead fissure of the 13X from soaking in water. After these treatments, the zeolite was washed with distilled water to remove fines. The 13X zeolite was then immersed into the silver nitrite ($AgNO_3$) solution of 1.2 N for 8 hours at room temperature, and washed with distilled water to remove the excess salt ions. The AgX was dried to obtain a constant weight in a vacuum oven at 180°C for 24 hours. The silver ion-exchanged amount of each AgX was obtained by the weight gains from the initial weight of 13X. Silver ions are included within the pore structure of the zeolite as isolated Ag^+ ions.

Fixed-Bed Adsorption and Desorption Experiment

A schematic diagram of the experimental apparatus is shown in Fig. 1. Gaseous methyl iodide is produced by evaporation of aqueous methyl iodide. The gas-phase concentration is adjusted by controlling the solution temperature and the nitrogen flow rate to methyl iodide generators. Dry air was used as a carrier gas at 4 l/min, with a linear velocity of 0.18 m/sec. All parts of the system, such as the adsorption column, mixing baffle and gas flow lines, were made of glass and pyrex to prevent plating-out of the elemental iodine and trapping of methyl iodide. The temperature inside the adsorbent was controlled up to 400°C by heating the column in an electric furnace. A constant amount of the adsorbent is packed in a column with a dimension of 0.022 m I.D. by 0.6 m length, and the adsorbents was thermally equilibrated with the gaseous-phase. The effluent concentration of methyl iodide from the column was analyzed by gas chromatography with

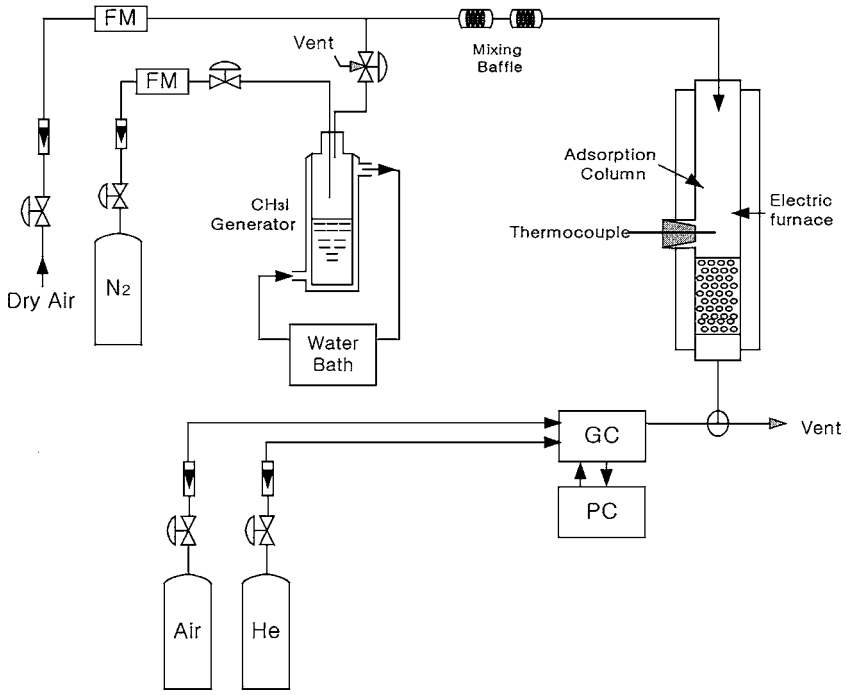

Figure 1. Schematic experimental apparatus for methyl iodide adsorption.

a pulse discharge detector (PDD) and GS-Q capillary column at an oven temperature of 140°C. Both the breakthrough curve of methyl iodide and the weight change of the adsorbent were used to obtain the adsorption amount of the adsorbate. Also, desorption after adsorption of methyl iodide was conducted by controlling the column temperature.

Results and Discussion

Uptake of Methyl Iodide in Terms of Temperature and Silver-Ion Loading

In a previous study (Choi et al., 1997), the adsorption capacities of methyl iodide on three kinds of base adsorbents, activated carbon, zeocarbon and 13X, were carried out at different temperatures from 30°C to 300°C. As shown in Fig. 2, activated carbon has excellent adsorption capacity at 30°C, however, the adsorption capacity markedly decreases as the temperature increases. On the other hand, 13X showed a higher adsorption capacity than activated carbon as the temperature increased. Zeocarbon shows a similar adsorption pattern to activated carbon at higher temperatures. Zeocarbon is composed of activated carbon (40 wt%)

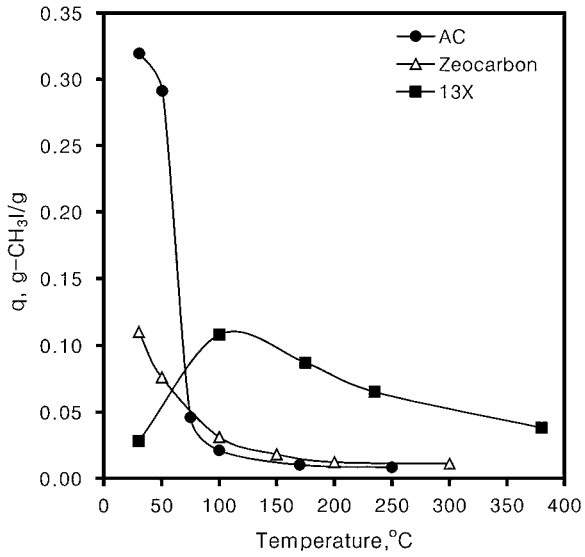

Figure 2. Adsorption amount of different base adsorbents (input conc. = 2.5×10^{-5} mol/L).

and zeolite 5A (60 wt%). This implies that a synergistic effect due to mixing of the two materials did not appear in the adsorption capacity. Contrary to activated carbon and zeocarbon, the increase in the adsorption capacity

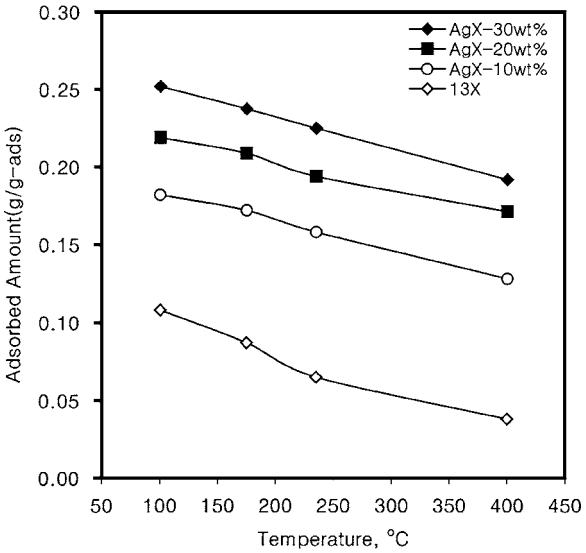

Figure 3. Adsorption amount of methyl iodide as a function of temperature and silver loading (input conc. $= 2.5 \times 10^{-5}$ mol/L).

of methyl iodide on 13X at higher temperatures up to 300°C is due to both physisorption and chemisorption occurring in the zeolite matrix. Thomas (1977) also reported that physisorption and chemisorption occurred simultaneously in zeolite. Based on the previous study, 13X zeolite is a reliable base adsorbent for the manufacture of a silver ion-exchanged adsorbent for the removal of methyl iodide at high temperatures.

In order to investigate the influence of silver-ion loading and temperature on the removal of methyl iodide, the adsorption of methyl iodide on the three kinds of AgX (10, 20, 30 wt%) were evaluated at four different temperatures (100, 175, 235, 400°C). The adsorption capacity decreases with increasing temperature and with decreasing silver content, as shown in Fig. 3. Since a higher silver level contributes to an increase of the number of Ag^+ ions, the chemical reaction between Ag^+ and CH_3I increased on silver ion-exchanged active sites. In general, a reduction of the micropore volume and partial blocking of the active site was observed with increasing silver ion-exchanged amounts. As listed in Table 1, however, the variation of the physical properties is small. The kinetic diameters of elemental iodine and methyl iodide are about 5 Å and 6 Å, respectively. The average pore diameters of base 13X and AgX are almost equal, approximately, 24 Å. Therefore, no partial blocking appeared to happen in the portion of unreacted silver sites in the matrix.

The previous studies reported the reaction between methyl iodide and silver on AgZ (Silver ion-exchanged mordenite) with the following equation (Jubin, 1994):

$$CH_3I + H_2O + Ag^{+} \rightarrow AgI + CH_3OH + H^+$$
$$CH_3I + CH_3OH + Ag^{+} \rightarrow AgI + CH_3OCH + H^+$$

However, the exact mechanism of the reaction between methyl iodide and AgX has not yet been reported. Based on a stoichiometric chemical reaction between methyl iodide and the amount of silver using the above equation, the percent silver utilization for the removal of iodide can be defined by the following equation.

$$\text{Silver Utilization Percent} = \frac{\text{Loading amount after desorption}(g-I/g-\text{adsorbent})}{\text{Removal amount by stoichiometric reaction}(g-I/g-\text{adsorbent})} \times 100$$

From the above definition, as shown in Fig. 4, the highest silver utilization percent was almost 100% for 10 wt% AgX obtained in the range of 150°C to 250°C, but a higher silver ion-exchange level yields lower silver utilization. From this result, it would be inferred that all silver-ions in the matrix of zeolite do not chemically react with methyl iodide as the silver ion-exchanged level increases. In the case of the results at 100°C, it is difficult to calculate the percent silver utilization because the loading amounts after desorption are very small due to physical adsorption. From the above experimental results, the optimal conditions for

Table 1. Physical properties of silver-exchanged zeolite.

	MS-13X (0 wt%)	AgX (10 wt%)	AgX (20 wt%)	AgX (30 wt%)
Average pore diameter (Å)	24.5	24.4	23.4	23.6
Surface area (m^2/kg)	7.99×10^5	7.95×10^5	7.20×10^5	6.99×10^5
Total pore volume (m^3/kg)	3.56×10^{-4}	3.22×10^{-4}	2.88×10^{-4}	2.81×10^{-4}
Micropore volume (m^3/kg)	2.37×10^{-4}	2.05×10^{-4}	1.92×0^{-4}	1.83×10^{-4}

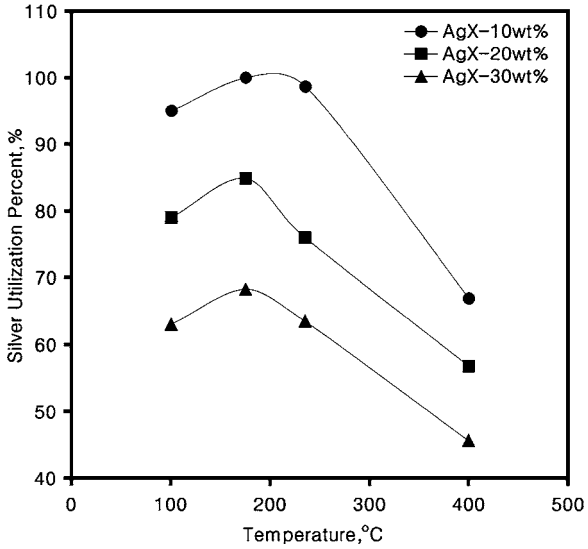

Figure 4. Evaluation for the utilization percent of silver.

the removal of methyl iodide are approximately 10 wt% of AgX and 175°C.

Characterization of Silver Ion-Exchanged Zeolites

In order to investigate the physical and chemical properties of the base adsorbent, 13X and silver ion-exchanged zeolite, AgX, some instrumental analyses were conducted. The surface area and pore size distribution are the important physical properties and need to be known. They were measured by BET-N_2 analysis (Micromeritics, ASAP 2400) for both the base adsorbent and AgX. The surface area of AgX decreases slightly with an increasing amount of silver ion-exchange. The determined surface area was determined to be about 800 m^2/g and the average pore size is 24 Å. The physical properties are listed in Table 1. The pore size distribution of AgX was not much different from that of the base 13X zeolite, as shown in Fig. 5. Compared with activated carbon, zeolite has thermal stability at higher temperature. Figure 6 shows the thermal analysis for methyl iodide adsorbed on the 10 and 30 wt% AgX. The thermal stability of these zeolites is good up to 1,000°C. They also have an exothermic peak at around 350°C. In addition, an SEM-EDS analysis was conducted to investigate the ion-exchanged state between silver and the sodium of base 13X. As listed in Table 2, there was good agreement of the ion-exchange state between silver and sodium for 10 wt% and 30 wt% AgX, and also for 10 wt% AgX after the

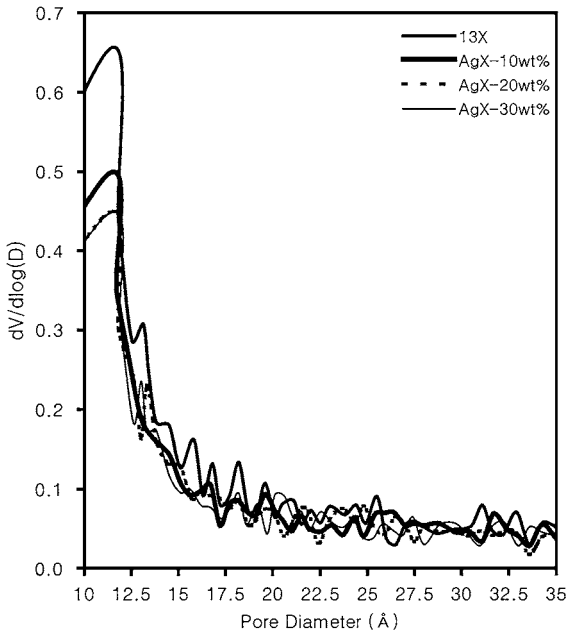

Figure 5. Pore size distribution of AgX in terms of silver loading.

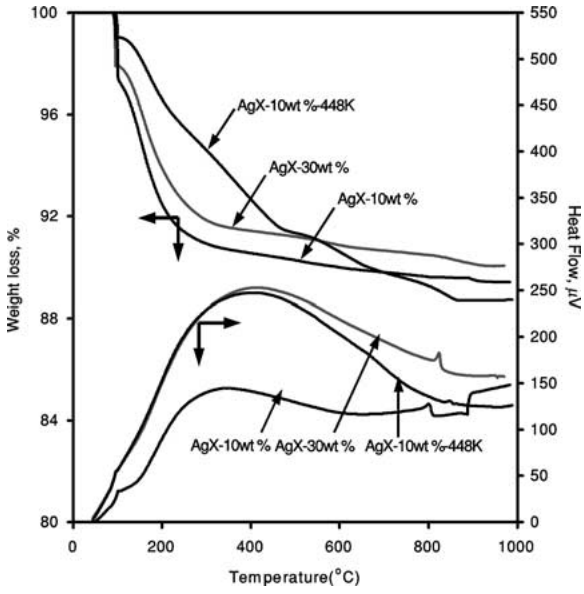

Figure 6. Thermal analysis of TG/DTA curves for 10 wt% and 30 wt% AgX.

adsorption of methyl iodide at 175°C. Figure 7 shows the SEM-EDS analysis for 10 and 30 wt% AgX and also for 10 wt% AgX after adsorption of methyl iodide at 175°C. It is thought that silver ions are well distributed without the formation of any large clusters or crystals of Ag metal or oxide.

Table 2. Element weight percent by SEM-EDS analysis for 10 and 30 wt% AgX.

Element	C	O	Na	Mg	Al	Si	Ag	I	Total
AgX10	9.45	42.69	7.05	1.20	10.99	17.04	11.37	–	100.0
AgX30	9.24	36.85	1.89	1.07	9.21	14.92	26.81	–	100.0
AgX10-175°C	7.50	38.47	5.32	1.35	9.65	15.11	10.54	12.07	100.0

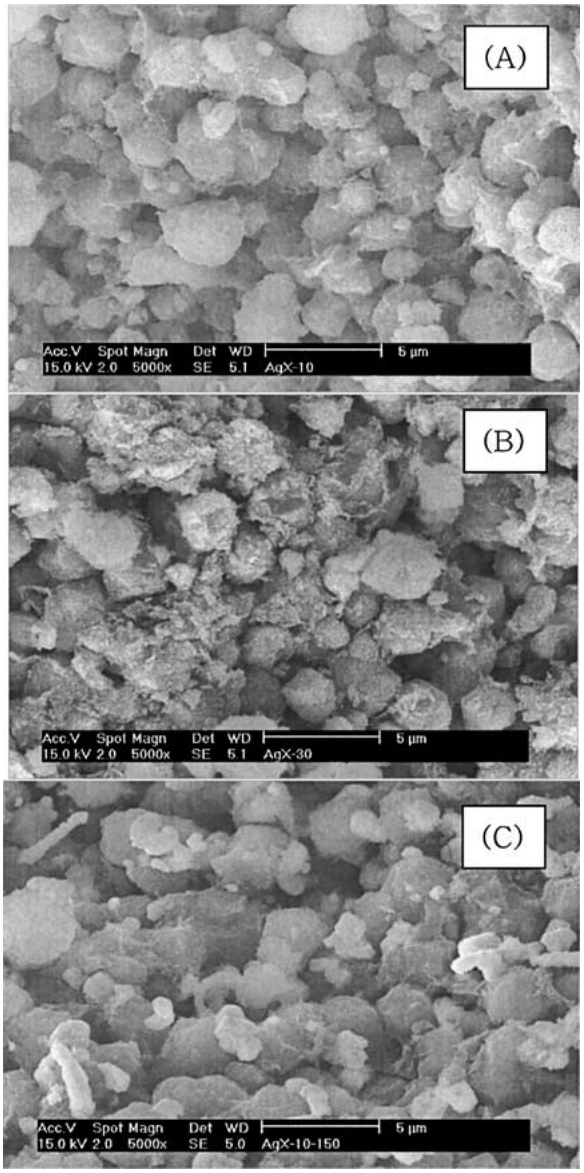

Figure 7. SEM-EDS analysis of 10 wt% and 30 wt% AgX; (A) AgX-10 wt%, (B) AgX-30 wt%, (C) AgX-10 wt%-175°C.

Adsorption Equilibrium

Isotherms play an important role in the prediction and design of adsorption systems. Thus, the careful selection of a single component isotherm depends on the concept of the accuracy and thermodynamic consistency of an isotherm model. The accuracy of an isotherm model is a function of the number of independent parameters. However, its popularity in relation to the process application is a function of mathematical simplicity. The Langmuir isotherm provides a somewhat less satisfactory fit compared to the Langmuir-Freundlich isotherm. The Langmuir-Freundlich equation provides a very close fit of the experimental data over its versatility in fitting the isotherms of various degrees of nonlinearity, which is important in multicomponent equilibrium prediction. Apart from its numerical aspect, the question of thermodynamic consistency of the model should also be addressed. Malek and Farooq (1997) reviewed a number of the important isotherm models. The following list gives the more pertinent characteristics of the isotherm models;

$$\left.\frac{\partial q}{\partial P}\right|_r \to \text{const.} \quad \text{as} \quad P \to 0 \tag{12}$$

$$q \to 0 \quad \text{as} \quad P \to 0 \tag{13}$$

$$q \to q_s \quad \text{as} \quad P \to \infty \tag{14}$$

The requirements of Eqs. (13) and (14) are not generally a problem. Unfortunately, the Langmuir-Freundlich equation does not reduce to Henry's law at low concentration. One may therefore question the reliability of this isotherm models in the low concentration region. However, the disadvantage of this limitation on a process application should be approached in relation to the overall effectiveness of alternative isotherm models, namely, the goodness-of-fit of the isotherm data and calculation time in a dynamic simulation.

The adsorption and desorption of methyl iodide on 10 wt% AgX were carried out in terms of four different temperatures (100, 175, 235, 400°C). A typical result of the total amount of adsorption, that is, the sum of both physisorption and chemisorption, on 13X at 175°C is shown in Fig. 8, with the simulated result fitted by the isotherm model. The total adsorption amount on 10 wt% AgX at different temperatures is also represented in Fig. 9. The Langmuir and Langmuir-Freundlich parameters of different temperatures are listed in Table 3.

Since most adsorption systems are thermodynamically exothermic processes, the heat effect should be examined, although the order of magnitude is somewhat different depending on the adsorption systems. In order to analyze nonisothermal adsorption processes quantitatively, the isotherm model should be correlated with temperature. In this study, two different models are selected, namely the Langmuir and Langmuir-Freundlich equations. Since the isotherm parameter, b, in both models is a function of temperature, the isotherm parameters listed in Table 4 were extracted simultaneously from all the sets of equilibrium data obtained at four different temperatures (100, 175, 235, 400°C) using multivariable, nonlinear regression. In this regard, a modified Levenberg-Marquardt algorithm was used (IMSL routine DUNLSF). Representative experimental data for the adsorption of methyl iodide on 10 wt% AgX at four different temperatures, along with their isotherm model fits, are shown in Fig 9. The thin and thick solid lines are the result simulated by using isotherm parameters listed in Table 3 and Table 4, respectively. The nonlinearity of the isotherm type in terms of temperature was almost similar, but the saturation amount was somewhat different. Adsorption breakthrough curves were simulated taking into account heat effects using the isotherm parameters listed in Table 4.

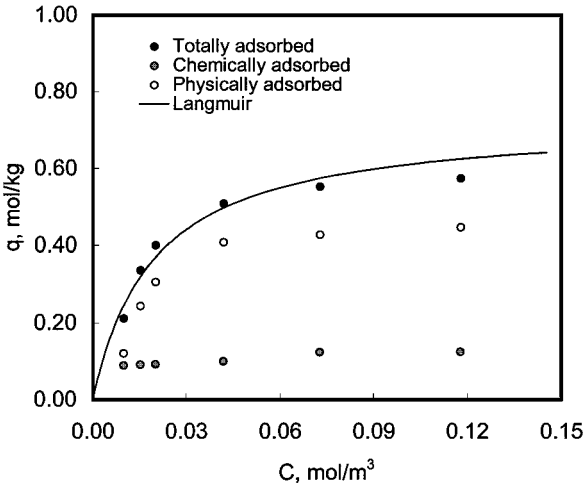

Figure 8. A typical adsorption and desorption of methyl iodide on 10 wt% 13× at 175°C.

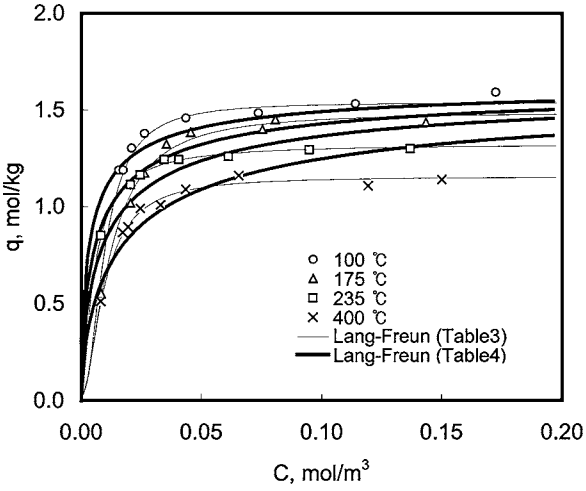

Figure 9. Adsorption isotherm of methyl iodide on 10 wt% AgX in terms of temperature.

Determination of Model Parameters

In a column packed with porous adsorbent, the major kinetic parameters are the axial dispersion coefficient, the axial thermal conduction coefficient, and the intraparticle diffusion coefficient. These parameters contribute to the broadening of the concentration profiles. The axial dispersion coefficient, D_L, was determined from the literature correlation given by Edwards and Richardson (1968). The molecular diffusivity, D_m, required in the Sherwood number, Sh, was calculated using the Fuller equation (Reid et al., 1987). For the energy equation, the effective axial thermal conductivity, K_L, was estimated using the empirical correlation given by Kunii and Smith (1960) and Yagi et al. (1960). The gas viscosity and thermal conductivity in the column were calculated as a mixture of the inert carrier and the sorbate, using the semiempirical formulas of Wilke (Bird et al., 1960). The gas density and specific heat capacity were calculated based in a weighted average of the carrier sorbate. The LDF coefficient, α, which lumps together the external and internal mass transfer resistances, was determined by comparing the experimental concentration profile with predictions based on

Table 3. Isothermal model parameters of methyl iodide on silver-exchanged zeolites (AgX 10 wt).

Model	Parameter	Temperature			
		100°C	175°C	235°C	400°C
Langmuir	q_m	1.6519	1.5627	1.3699	1.2623
	b	1.648×10^2	1.200×10^2	2.195×10^2	1.094×10^2
Langmuir-Freundlich	q_m	1.5405	1.4928	1.3258	1.1564
	b	9.608×10^3	1.485×10^3	0.929×10^3	3.467×10^3
	n	5.07×10^{-1}	6.09×10^{-1}	7.68×10^{-1}	5.73×10^{-1}

Table 4. Langmuir and Langmuir-Freundlich parameters taking into account heat effect for methyl iodide on 10 wt% AgX.

Model	Langmuir			Langmuir-Freundlich			
Parameters	q_m	b_0	$-\Delta H_A$	q_m	b_0	$-\Delta H_A$	n
Values	1.432	0.369	2.369×10^4	2.203	0.344	7.286×10^3	5.156

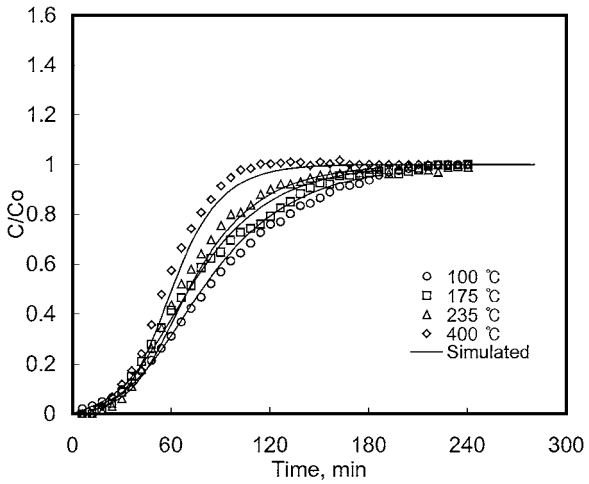

Figure 10. Experimental and theoretical breakthrough curves for methyl iodide in terms of temperature at $L = 2.6$ cm.

the proposed model. Figure 10 shows the experimental concentration profiles according to the four different temperatures at a short column, $L = 2.6$ cm, with those fitted by the proposed model. The solid line represents the model prediction obtained by adjusting the value of the LDF coefficient. The experimental conditions and the determined model parameters are listed in Table 5 and Table 6, respectively.

Simulation of Adsorption Breakthrough Curves

The performance and operating cost of an adsorption-based removal process greatly depend on the effectiveness and operating conditions. Therefore, rigorous approaches to the design and operation of the adsorption system must be used to ensure efficient and cost effective applications. To do this, one has to understand the mechanism and dynamics of adsorption as well as the major variables, which affect the process performance. In general, adsorption equilibrium, external and internal mass transfer, and hydrodynamics are needed to simulate adsorption behavior in a fixed-bed adsorber. When thermal effects can't be ignored in an adsorption system, they should be considered in model formulation.

Figures 11 and 12 show the experimental breakthrough curves in a deep bed length at $L = 10$ cm to compare the influence of thermal effects. The solid

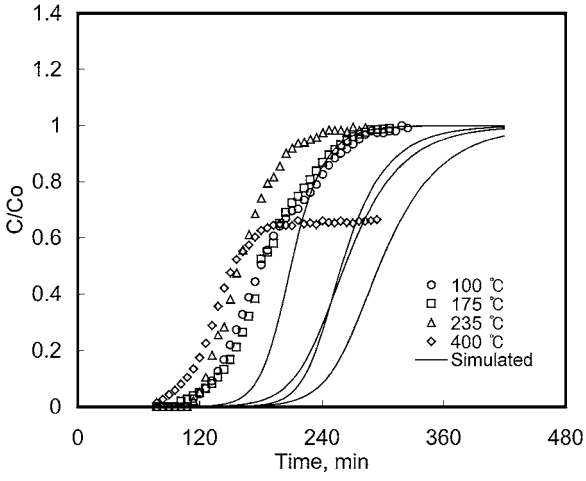

Figure 11. Experimental and theoretical breakthrough curves simulated by isothermal adsorption model for methyl iodide at $L = 10$ cm.

Table 5. Properties of the adsorbent and other experimental information.

Column	Jacket glass Internal diameter Length	2.2 cm 2.6, 10 cm
Adsorbent		Silver-exchanged zeolite
	Apparent density	1532 kg/m^3
	Particle porosity	0.31
	Mean pore diameter	24.4
	Specific surface area	795 m^2/g
	Heat capacity	0.837J/kg · K
	Size	8–16 mesh
	Bed porosity	0.46
Adsorbate	Heat capacity	CH_3I (100.0%) 29.0 J/mol · K
Carrier Experimental range		Air
	Gas velocity	4.0 L/min
	Pressure	1.0 bar
	Temperature	100, 175, 235, 400°C

Table 6. Model parameters for the simulation of breakthrough profiles.

Temp	D_m (m^2/s)	D_L (m^2/s)	k (1/s)	K_L (J/ms · K)
100°C	1.574×10^{-4}	1.175×10^{-4}	1.26×10^{-4}	2.929
175°C	2.168×10^{-4}	1.126×10^{-4}	6.33×10^{-4}	2.184
235°C	2.702×10^{-4}	1.087×10^{-4}	6.33×10^{-4}	1.802
400°C	4.419×10^{-4}	0.992×10^{-4}	1.26×10^{-4}	1.156

lines in Figs. 11 and 12 represent simulated results based on the isothermal and nonisothermal adsorption equilibrium models, respectively. The equilibrium model parameters were listed in Table 3 and Table 4, respectively. From this result, the heat effect due to exothermic reaction in the deep bed should be accounted for, compared to the one in a shallow bed. However, the magnitude of that heat effects is not seen to be high as shown in Fig. 12 with temperature profiles. In particular, the breakthrough curve for the longer bed at 400°C showed abnormal behavior. This result has not been reported so far. In similar previous studies (Jubin, 1994; Modolo and Odoj, 1997; Funabashi et al., 1995; Thomas et al., 1977), the removal efficiency mainly focused on the breakthrough time to reach a permissible effluent concentration, not on the saturation capacity. Two explanations can be given for this result. One is the concept of the catalytic decomposition of CH_3I by the AgX adsorbent. Another is due to the longer contact time than that of the shallow bed. It may be considered that a portion of the methyl iodide supplied from bed inlet decomposes to a hydrocarbon, such as $C_xH_y + I_2$ on the AgX adsorbent. From the standpoint of CH_3I inventory, after the bed reached its saturation limits, the expected "in = out" mass balance was not observed due to catalytic decompositions. In this regard, CH_3I was dissociated as $CH_3{}^+$ and I^- on the silver loaded zeolite surface to first form silver iodide by chemisorption and to produce C_xH_y species. From this result, it seems that a portion of reacted silver iodide as well as silver acts as a catalyst for CH_3I decomposition as well as a stable compound. Various metal ion-exchanged or impregnated zeolite catalysts have been tested, and metal ions such as Co^{2+}, Mn^{+2}, Ni^{-2}, Ag^+, etc. have been identified as active for selective catalytic reduction of nitric oxide by methane over the zeolites (Liu et al., 1999; Li and Stephanopoulos, 1997). It may be considered that Ag-loaded zeolite has a dual function: Ag ions, one of the best cations for π-complexation with π-electrons, supply active sites for the reaction between methyl iodide and silver, and act as a catalyst of CH_3I decomposition. In our laboratory, some

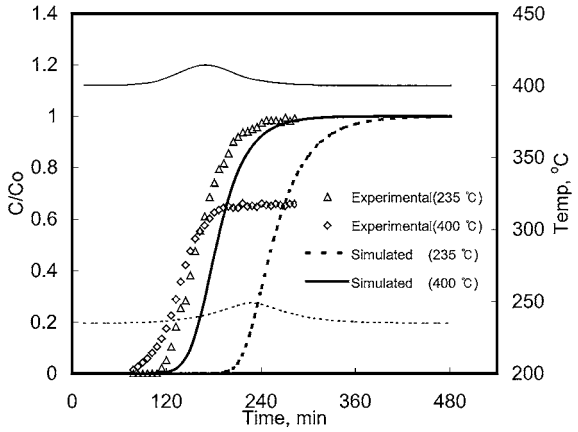

Figure 12. Experimental and theoretical breakthrough curves simulated by nonisothermal adsorption model for methyl iodide at $L = 10$ cm.

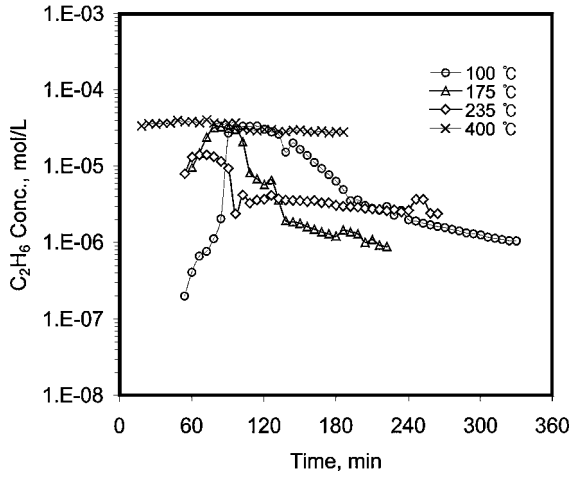

Figure 13. Concentration profiles of C_2H_6 in a 10 wt% AgX column at $L = 10$ cm and $T = 400°C$.

efforts have been focused to reveal the reaction mechanism for this result. Figures 13 and 14 show the experimental concentration profiles of methane and carbon dioxide simultaneously measured with methyl iodide. Although no precise reaction mechanism could be proposed from the experimental data obtained so far, the following mechanism can be assumed:

$$2CH_3I + 2Ag \rightleftarrows 2AgI + C_2H_6 \quad \text{or}$$
$$2CH_3I + 2Ag + 1/2O_2 \rightleftarrows 2AgI + CH_3OCH_3$$

From the photographic evidence shown in Fig. 7, silver ions and/or metal oxides are included within the

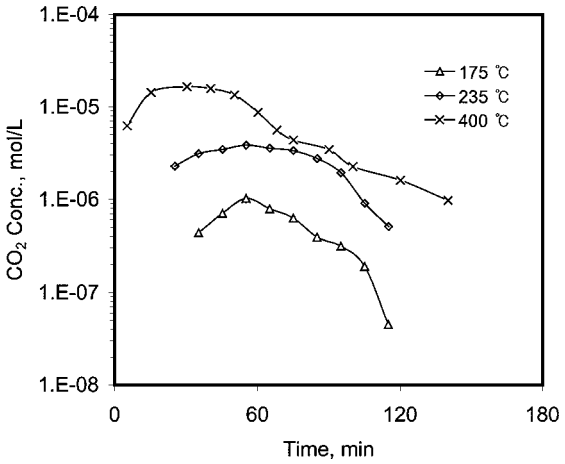

Figure 14. Concentration profiles of CO_2 in a 10 wt% AgX column at $L = 10$ cm and $T = 400°C$.

pore structure of the zeolite as isolated Ag^+ ions. As the iodine loaded onto the AgX, the material became yellow and it was getting deeper yellow as more iodine was trapped at higher temperature. It is reported that from the results of XAFS and DRS measurement, silver ions are anchored onto the inner surfaces of the micropores of the zeolite in a highly dispersed state without or possibly the formation of any large clusters or crystals of Ag metals or oxides (Jubin, 1994). The surface chemistry reported here for methyl iodide adsorbed on Ag–loaded zeolite surfaces show a great similarity with that seen in other systems, especially on Ni-loaded surfaces. Previous studies showed that low-temperature chemisorption of alkyl iodides on metal substrates is molecular and through iodine atoms. They have also showed that, at temperatures around 150–200 K, the C—I bond dissociates in a reaction that requires an activation energy of only about 5 kcal/mole, which generates iodine atoms and alkyl species on the surface (Liu et al., 1999). Although there is a lack of spectroscopic data for the identification of the surface species that form during the thermal activation of methyl iodide on the Ag surface, it is quite reasonable to expect the C—I bond to break first and to form silver iodide on this surface as well. For continuous work to verify reaction mechanism, further studies will be done and reported within near further.

Concluding Remarks

Adsorption equilibrium and dynamics were studied for the removal of methyl iodide using various silver

ion-exchanged zeolites in a column adsorber under operating conditions such as temperature and methyl iodide concentration. The optimal silver ion-exchanged amount and temperature were about 10 wt% and 175°C, respectively. A simple dynamic model formulated by employing the linear driving force(LDF) approximation inside the adsorbents and the nonisothermal Langmuir-Freundlich isotherm equation, simulated the experimental breakthrough curves in terms of temperature, 100, 175, 235, 400°C. The agreement of the prediction of breakthrough curves of methyl iodide by the nonisothermal model was somewhat better(except for those obtained at 400°C), compared with the isothermal model. However, catalytic reaction should be incorporated in the proposed model to more precisely simulate the breakthrough curves obtained in a deep bed at high temperature. This will be continued together with work for the verification of the reaction mechanism and the reaction constants of methyl iodide on a silver ion-exchanged zeolite surface.

Notation

b_0 constant in the Langmuir-Freundlich equation (1/bar)
C_T total gas-phase concentration in the bed (mol/m^3)
C_f gas-phase concentration of the adsorbate in the feed (mol/m^3)
C_{pg} gas heat capacity (J/mol·K)
C_{ps} particle heat capacity (J/kg·K)
d_f mean particle diameter (m)
D_m molecular diffusivity (m^2/s)
D_L axial dispersion coefficient (m/s)
k LDF coefficient (1/s)
K_g axial gas-phase thermal conductivity (J/m · s · K)
K_L effective axial thermal conductivity (J/m·s·K)
K_p particle thermal conductivity (J/m · s · K)
L column length (m)
n constant in the Langmuir-Freundlich equation (1/ bar)
m adsorbent weight
P pressure (bar)
P_e Peclet number $(v_f d_p)/D_L$
P_r Prandtl number $(\frac{(C_{pg})\mu}{K_g})$
q adsorbed phase concentration (mol/kg)
q^* equilibrium adsorbed phase concentration (mol/kg)
q_s^* saturated equilibrium adsorbed phase concentration (mol/kg)
R universal gas constant (J/mol.K)
Re Reynolds number
Sh Sherwood number
Sc Schmidt number $(\mu D_m/\rho_g)$
T temperature (K)
t time (s)
v velocity (m/s)
V dimensionless velocity (v/v_f)
X dimensionless sorbate mole fraction of gas phase (C/C_f)
Y dimensionless solid-phase concentration (q/q_s^*)
z space dimension (m)

Greek letters

α dimensionless constant (Lk/v_f)
χ dimensionless constant (z/L)
ε void fraction
ϕ dimensionless constant $(C_T C_{pg}/(C_T C_{pg} + m\rho_p C_{ps}))$
φ dimensionless constant $((1-\varepsilon_B)/\varepsilon_B(q_s^*/C_t)\rho_p)$
μ viscosity
θ dimensionless temperature (T/T_f)
ρ density (g/cm^3)
τ dimensionless time $(v_j t/L)$.
ζ dimensionless constant $(-\Delta H_A)/C_{pg}T_f$

Superscripts and subscripts

b bed
n exponent in the single-component Langmuir-Freundlich isotherm
e bed exit condition
f feed or inlet conditions
g gas phase
o initial conditions
p particle
T total

Acknowledgment

This project has been carried out under the Nuclear R&D Program by MOST

References

Bird, R.B., W.E. Stewart, and E.N. Lightfoot, *Transport Phenomena*, Wiley, New York, 1960.

Reid, R.C., J.M. Prausnitz, and B.E. Poling, *The Properties of Gases and Liquids*, McGraw-Hill, New York, 1986.

Choi, B.S. and G.I. Park, "A Study on the Removal of Radioiodine on Silver-Exchanged Adsorbents," in *Proc. of the KNS Autumn Meeting*, 311–316 (1997).

Deitz, V.R. and L.A. Jonas, "Catalytic Trapping of Methyl Iodide by Beds of Impregnated Charcoal," *Nuclear Technology*, **37**, 59–64 (1978).

Edwards, M.F. and J.F. Richardson, "Gas Dispersion in Packed Beds," *Chem. Eng. Sci.*, **23**, 109–115 (1968).

Finlayson, B.A., *The Method of Weighted Residuals and Variational Principles*, Academic Press, New York, 1972.

Funabashi, K., T. Fukasawa, and M. Kikuchi, "Investigation of Silver-Impregnated Alumina for Removal of Radioactive Methyl Iodide," *Nuclear Technology*, **109**, 366–372 (1995).

Jubin, R.T., "The Mass Transfer Dynamics of Gaseous Methyl Iodide Adsorption by Silver-Exchanged Modernite," Ph.D. Thesis, The University of Tennessee, Knoxville, USA, 1994.

Kovach, J.L., "The Environment and Current States of Radioiodine Control", in *Proc, 16th Nuclear Air Cleaning Conf.*, San Diego, California, October 20–23, 1980, CONF-801038, U.S. Department of Energy, 417–428 (1981).

Li, A. and M.F. Stephanopoulos, "Selective Catalytic Reduction of Nitric Oxide by Methane over Cerium and Silver Ion-Exchanged ZSM-5 Zeolite," *Applied Catalysis A*, **165**, 15–34 (1997).

Liu, C.J., R. Mallinson, and L. Loggan, "Comparative Investigation on Plasma Catalytic Methane Conversion to Higher Hydrocarbons over Zeolite," *Applied Catalysis, General*, **178**, 17–27 (1999).

Malek, A. and S. Farooq, "Comparison of Isotherm Models for Hydrocarbon Adsorption on Activated Carbon," *AIChE J.*, **42**(11), 3191–3201 (1996).

Marin, F.C., M.D. Garcia, I.F. Morales, and F.J.L. Garzon, "Dynamics Adsorption of Methyl Iodide on Activated Carbon," *Carbon*, **29**, 629–634 (1991).

Modolo, G. and R. Odoj, "Investigation on the Partitioning of I from Silver-impregnated Silica in Preparation for Further Transmutation," *Nuclear Technology*, **117**, 80–86 (1997).

Pence, D.T. and B.A. Staples, "Solid Adsorbents for Collection and Storage of Idoine-129 from Reprocessing Plants," in *Proc. 13th AEC Air Cleaning Conf.*, CONF-740807, 758–764 (1974).

Raghavan, N.S. and D.M. Ruthven, "Numerical Simulation of a Fixed Bed Adsorption column by the Method of Orthogonal Collocation," *AIChE J.*, **29**(6), 922–928 (1983).

Ruthven, D.M., S. Farooq, and K.S. Knaebel, *Pressure Swing Adsorption*, VCH, New York, 1994.

Ruthven, D.M., *Principles of Adsorption and Adsorption Process*, Wiley, New York, 1984.

Thomas, T.R., B.A. Staples, L.P. Murphy, and J.T. Nichols, "Airborne Elemental Iodine Loading Capacities of metal Zeolites and a Dry Method for Recycling Silver Zeolite," in *Proc. 14th ERDA Air Cleaning Conference*, CONF-760822, 363–380 (1997).

Villadsen, J. and M.L. Michelsen, *Solution of Differential Equation Methods by Polynomial Approximation*, Prentice-Hall, Englewood Cliffs, 1978.

Wren, J.C., C.J. Moore, and M.T. Rasmussen, "Methyl Iodide Trapping Efficiency of Aged Charcoal Samples from Bruce—A Emergency Filtered Air Discharge Systems," *Nuclear Technology*, **125**, 28–39 (1999).

Yagi, S., D. Kunii, and N. Wakao, "Studies on Axial Effective Thermal Conductivities in Packed Beds," *AIChE J.*, **6**(4), 543–548 (1960).

Yang. R.T., *Gas Separation by Adsorption Processes*, Butterworths, Boston, 1987.